ORIGINAL ARTICLE

Multi-objective optimisation of fused filament fabrication of acrylonitrile butadiene styrene for enhancing mechanical performance and build time

Phan Quoc Khang Nguyen[1] · Yixia Sarah Zhang[1] · Zhongpu Zhang[1] · Richard Chunhui Yang[1]

Abstract

Fused filament fabrication (FFF), a 3D printing technique, has gained prominence due to its diverse application in rapid prototyping, custom tooling, architectural modelling, and medical device fabrication. The current literature shows extensive works on single-objective optimisation but limitation in studies on multi-objective optimisation that determines a set of process parameters to attain a balance between conflicting properties such as mechanical properties and build time. Therefore, this study experimentally investigates mechanical properties and build time of FFF printed acrylonitrile butadiene styrene (ABS), considering the influences of five key FFF printing process parameters on mechanical properties, including extrusion temperature, layer thickness, printing speed, number of contours, and infill density. Response surface methodology (RSM) and artificial neural network (ANN) are both adopted for pattern recognition before the genetic algorithm (GA) and multi-criteria decision-making (MCDM) algorithm are applied for optimisation. Results reveal that the infill density is the main contributor to tensile strength while the layer thickness has the highest impact on build time. Both RSM-GA and ANN-GA approaches succeed at achieving a balance between tensile strength and build time. In comparison to RSM, ANN proves to be a superior tool with remarkable accuracy in predicting responses across diverse parameter settings. The findings of this study hold significant implications for designers and manufacturers of domestic and small industrial components.

Keywords Acrylonitrile butadiene styrene (ABS) · Build time · Fused filament fabrication (FFF) · Machine learning · Mechanical properties · Multi-objective optimisation

1 Introduction

Additive manufacturing (AM), also known as 3D printing, is a revolutionary manufacturing process to build objects layer by layer from digital designs. Unlike traditional subtractive technology involving material removal, AM adds material only where it is needed, resulting in reduced waste and intricate geometries for sustainability [1, 2]. During the COVID-19 pandemic, AM emerged as a vital tool in addressing supply chain disruptions and urgent medical equipment shortages, and AM technologies were rapidly deployed to produce personal protective equipment (PPE) such as face shields, ventilator components, and nasal swabs. The flexibility of 3D printing allowed for quick design iterations and localised production, enabling healthcare facilities and communities to respond to the crisis by producing essential items on-site [3]. Fused filament fabrication (FFF) is a material extrusion-based AM technique that constructs objects by melting and extruding thermoplastic filaments layer by layer. Widely known for its accessibility and versatility, FFF technique is used in various industries for rapid prototyping, functional part production, and educational purposes. Currently, FFF holds significant value in the circular economy due to its role in sustainable manufacturing. For example, by utilising both mechanically and chemically recycled plastics, FFF minimises waste, conserves resources, and extends the life of polymers.

The optimisation of the FFF printing process parameters is crucial for achieving consistent and high-quality FFF-printed objects. Properly calibrated parameters, such as layer thickness, printing speed, extrusion temperature,

✉ Richard Chunhui Yang
R.Yang@westernsydney.edu.au

1   Centre for Advanced Manufacturing Technology, School of Engineering, Design and Built Environment, Western Sydney University, Locked Bag 1797, Penrith, NSW 2751, Australia

and infill density, ensure optimal bonding between layers and mechanical properties [4, 5]. This precision minimises print failures, reduces material waste, and enhances production efficiency. Surface roughness, mechanical strength, and dimensional accuracy are key attributes frequently targeted for optimisation in FFF, ensuring that FFF printed parts exhibiting desired aesthetics, structural integrity, and precise dimensions. The layer thickness, extrusion temperature, printing speed, and raster width were found as the key FFF printing process parameters contributing to surface roughness (SR), build time (BT), and volume percentage error (VPE). Via using artificial neural networks (ANN) and the whale optimisation algorithm for optimisation, the layer thickness was found to be the most significant factor for SR, BT, and VPE [6]. A different study confirmed the increase of layer thickness strongly impacted all surface parameters of FFF-ed parts made of ABS [7]. Multiple machine learning models were employed to evaluate the nonlinear effects of layer thickness, printing speed, number of contours (also known as number of shells), build orientation and extrusion temperature on the surface roughness of polyvinyl butyral (PVB), and layer thickness and build orientation were found having the highest impact on the surface roughness [8]. The effects of all 13 FFF printing process parameters on the dimensional accuracy and geometric characteristic of FFF printed parts were investigated, and the number of contours was concluded as the most influential factor for dimensional accuracy while layer thickness had the highest contribution to geometric characteristics [9]. In another study [10], after the specimens were fabricated under the variation of layer thickness, build orientation, infill density, and number of contours, the response surface methodology (RSM) and ANN were adopted to study the nonlinearity of the data before optimising the part properties using genetic algorithm (GA). Tensile strength (TS) stands as a paramount consideration in optimising mechanical performance within FFF [11, 12]. This property, reflecting a material's resistance to the applied forces, plays a pivotal role in determining the durability and load-bearing capacity of 3D-printed objects, thereby guiding the refinement of FFF parameters to attain enhanced structural integrity. Layer thickness, air gap, raster width, build orientation, raster angle, and number of contours were taken into account to optimise TS, SR, and BT of FFF printed parts, and their results indicated that the longitudinal build orientation, less layer thickness, and greater raster width can improve material strength [13]. Another study confirmed that lower thickness enhanced mechanical responses and ANN model illustrated high accuracy in capturing the influences of layer thickness, raster angle, and printing speed [14]. When analysis of variance (ANOVA) and RSM were applied to understand the effects of layer thickness, infill density, and raster angle on mechanical properties, infill density was claimed to be the most significant

factor for improving TS, yield strength, elastic strength, and fracture strength [15].

While ANN has been utilised to capture the intricate nonlinear interactions between material properties and diverse process parameters, the quest to identify the optimal model persists as a manual undertaking. For instance, Vijayaraghavan, Garg [16], determined the best model after assessing varied structures with hidden layers ranging from 1 to 4 and neurons from 2 to 9 per layer. Similarly, Chinchanikar, Shinde [17], sought the optimal model, employing a maximum of three hidden layers and diverse neurons (10 to 750), yielding a correlation coefficient of 0.875 and an R-squared value of 0.765. Tayyab, Ahmad [18], optimised their ANN model for flexural strength using two hidden layers and a Bayesian algorithm. Alafaghani, Ablat [19], adopted a more exhaustive approach, exploring a wide range of combinations in hidden layers (1 to 2), neurons (3 to 10), and transfer functions. Their procedure resulted in 36 models, their final prediction being an average of all outputs, showcasing the intricate process of refining ANN models.

Although the aforementioned trial-and-error methods may be apt for scenarios involving a limited count of process parameters, they encountered challenges when faced with a greater number and intricacy of data points. As an illustration, Tura, Lemu [20], effectively established an ANN model, yielding a remarkable correlation coefficient R of 0.99 to predict tensile strength from merely three process parameters and 15 experimental data points. However, when confronted with an analogous quantity of process parameters and an expanded dataset of 30 experimental runs, the R coefficient dropped to 0.97 during the construction of the ANN to capture tensile strength trends [21]. Consequently, it is plausible to contend that a more comprehensive technique for constructing ANN should be devised through the evolution of contemporary software, replacing the manual selection process predominantly reliant on researchers' expertise.

Multi-objective optimisation in FFF holds a distinct advantage over single-objective optimisation by considering a broader range of factors simultaneously. While single-objective optimisation may focus solely on one aspect, such as tensile strength or material usage, multi-objective optimisation balances multiple factors like strength, surface finish, and time efficiency. This holistic approach results in more well-rounded solutions that cater to real-world complexities and trade-offs, leading to 3D-printed parts that excel across various criteria and better align with complex design requirements and manufacturing constraints. Gurrala and Regalla [22] performed multi-objective optimisation for the TS and volume shrinkage of FFF parts by controlling the model interior, horizontal direction, and vertical direction. Non-dominated sorting genetic algorithm II (NSGA-II) is a popular multi-objective optimisation algorithm known for its ability to efficiently handle complex problems

involving conflicting objectives [23]. In a study, NSGA-II was deployed to maximise the TS and minimise volume shrinkage. Apart from NSGA-II, bacterial foraging optimisation (BFO) and particle swarm optimization (PSO) are both nature-inspired optimisation algorithms, with BFO mimicking bacterial foraging behaviour [24] and PSO simulating the social behaviour of particles [25], and they can be effectively combined in hybrid models to leverage the strengths of both methods for more efficient optimization. In a literature [26], based on the Taguchi array, the effects of layer thickness, support material, model interior, and orientation were experimentally examined and multi-objective optimisation was performed for hardness, tensile strength, flexural modulus, and surface quality. All the responses were merged with suitable weight into a single response for PSO, BFO, and hybrid PSO-BFO. The technique for order of preference by similarity to ideal solution (TOPSIS) is a decision-making method used to evaluate and rank a set of alternatives based on multiple criteria [27]. In the context of FFF, TOPSIS holds importance as it enables a systematic approach to assess and select optimal combinations of process parameters for 3D printing. By considering various factors such as surface finish, mechanical properties, material usage, and printing time, TOPSIS aids in identifying the most suitable parameter settings that strike a balance between competing objectives. Dev and Srivastava [28] applied TOPSIS to conduct a multi-objective optimisation for TS, flexural strength (FS), and material weight (MW). The experiment was planned based on central composite design (CCD) and the controlled process parameters are layer thickness, raster angle, extrusion temperature, printing speed, and infill density. ANOVA results indicated the infill density as the highest influential factor for all responses. The sequential results of ANN-GA-TOPSIS were found to improve the TS, FS, and MW by 6.45%, 4.19%, and 11.47%. In another study, the TOPSIS played an important role in determining the optimal process parameters for TS and impact strength when the FFF parts were fabricated under the variation of layer thickness, infill density, and build orientation. Those results also revealed the increase of FS relative to the increase in layer thickness and infill density [29].

Despite the growing interest in FFF, there keeps a substantial blank in the exploration of multi-objective optimisation tailored to this additive manufacturing process. Notably, the existing literature lacks comprehensive investigations into the intricate interplay between build time and material performance within FFF-printed parts. Recognising the symbiotic relationship between material performance and build time is paramount to ensure a balanced approach that not only elevates high performance but also maintains the essential agility and competitiveness that FFF offers. Although the number of contours, referring to the outer perimeter lines printed around each layer of a 3D object,

was proved to enhance the material performance, e.g. tensile strength, its impact when correlated to other process parameters such as layer thickness, printing speed, extrusion temperature, and infill density on build time remains uncertain and inadequately explored [30, 31].

In this study, the objectives are outline as follows:

- The primary objective is to conduct a comprehensive multi-objective optimisation study targeting the simultaneous enhancement of build time efficiency and tensile strength in FFF printed acrylonitrile butadiene styrene (ABS).
- The second objective is to elucidate the influence of key FFF printing process parameters on tensile strength and build time.
- The third objective is to evaluate the ability of two models, RSM, and ANN, in predicting the properties with limited available data.

However, our current study is limited to perform multi-objective optimisation for only 5 key parameters. Moreover, our study focuses on enhancing one dimension of part qualities such as tensile strength while other qualities such as surface roughness and dimensional accuracy can be affected. The paper is outlined as follows. Section 2 focuses on the development of experimental, mathematical analysis, and optimisation procedures; Section 3 presents the obtained results and conducts the discussion; Section 4 presents the results of multi-objective optimisation and experimental validation; Section 5 analyses the internal structures and fractography of samples; and Section 6 draws conclusions based on the research findings and recommends the future work.

2 Materials and methodology

2.1 Development of three-stage material optimisation framework for FFF-printed ABS

In this study, a three-stage integrated experimental and theoretical analysis and optimisation framework for optimising FFF printed ABS is developed as depicted in Fig. 1.

At stage 1, the experiment was carried out using Taguchi array L27 to collect data on tensile strength and build time of printed samples. Then, the data set of 27 data points was utilised to train ANN and RSM models for comparative analysis. After that, additional experiments were carried out to evaluate the efficiency of the models and their potentials in practical applications. It was worth noting that a distinct predictive model was constructed for each response (either tensile strength or build time). At stage 2, GA and TOPSIS were adopted to generate optimal solutions using the devised predictive models built in the previous stage. The

Fig. 1 Schematic of systematic experimental and theoretical analysis framework for extracting material properties and optimisation
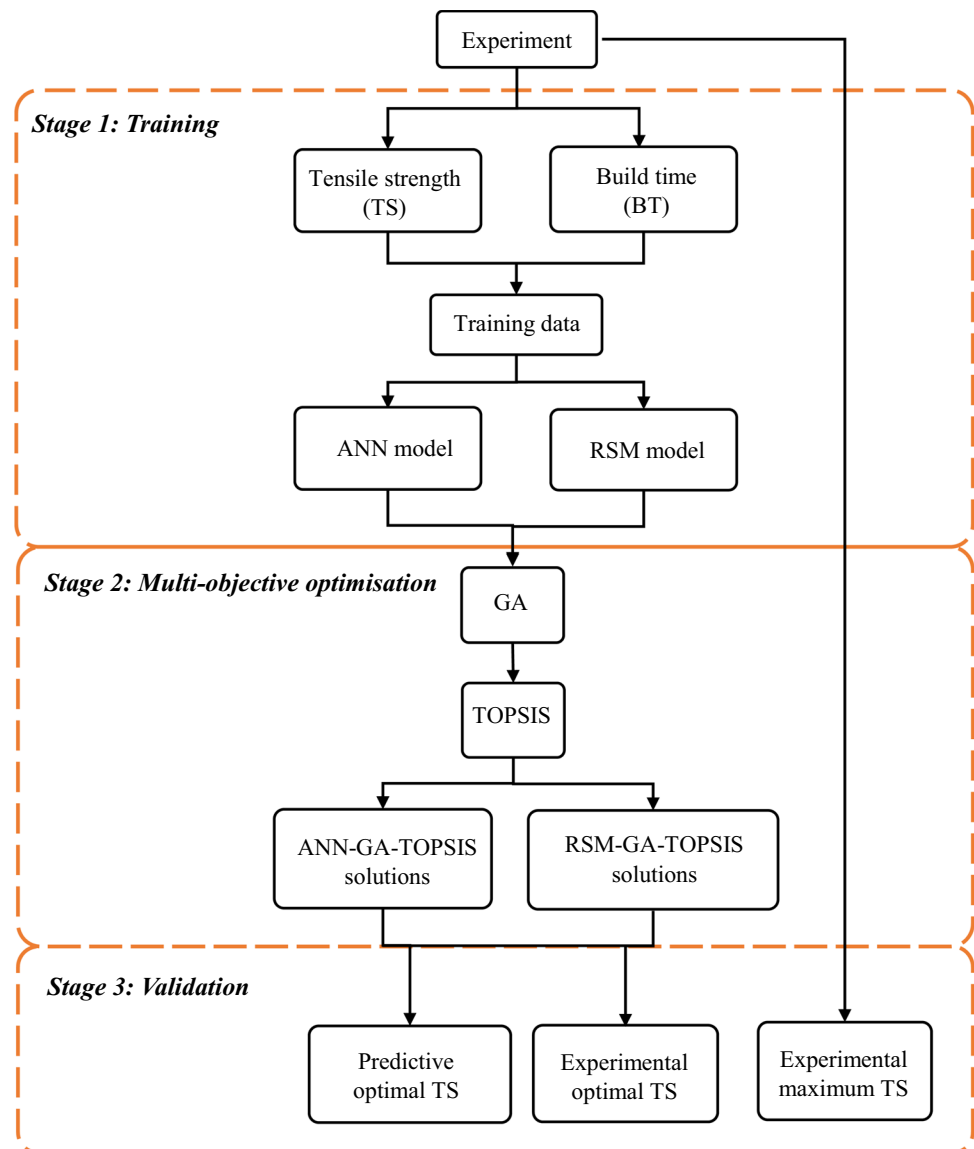
main target was to maximise the tensile strength while minimising build time. At stage 3, additional experimental work was performed, and validation was performed to evaluate the efficiency of the devised predictive models. Specifically, the effectiveness of each model (ANN-GA-TOPSIS and RSM-GA-TOPSIS) was determined by comparing the values of the prediction and experiment. After that, the experimental values of the optimal sets were compared with the maximum strength found from the original experimental set. Optimal set of the FFF printing process parameters was then determined based on the balance between the reliability of the predictive model and improvement.

2.2 Sample design and experimental procedures

The testing specimens utilised in this study were dog-bone shaped type-V specimens with a cross-sectional area of 3.18×3.20 mm, as outlined by the ASTM D638 standard. The CAD models of the specimens were created using SolidWorks and then imported into an FFF printer – Flashforge Creator 3 Pro for their 3D printing. The primary material employed for the 3D printing process was ABS purchased from Fillamentum with a filament tensile strength of 39 MPa.

The experimental design for this study was structured using the Taguchi L27 orthogonal array. Taguchi arrays are orthogonal designs used in robust design experiments to systematically study the effects of multiple factors with minimal trials. The L27 array is a 3^3 design, meaning that it consists of 27 experimental runs, supports up to 13 factors at 3 levels each, and allows for analysing 5 factors at 3 levels while maintaining orthogonality across selected factors [32]. The goal was to comprehensively analyse the effects of five key FFF printing process parameters, which are the extrusion

Table 1 FFF varied process parameters and their levels

Parameter	Notation	Units	Number of levels	Level 1	Level 2	Level 3
Extrusion temperature (ET)	X_1	°C	3	234	237	240
Layer thickness (LT)	X_2	mm	3	0.1	0.2	0.3
Printing speed (PS)	X_3	mm/s	3	40	70	100
Number of contours (NC)	X_4	-	3	1	2	3
Infill density (ID)	X_5	%	3	40	70	100

Table 2 FFF fixed process parameters

Parameter	Units	Value
Build orientation	-	Longitudinal
Raster angle	-	0°/90°
Fan speed	%	15
Nozzle diameter	mm	0.4
Platform temperature	°C	100
Retraction speed	mm/s	30 mm/s
Fill pattern	-	Line
Cross angle	-	90°

temperature, infill density, layer thickness, printing speed, and number of contours. Each parameter was varied at three distinct levels as shown in Table 1 and their ranges were suitably determined from printing trials. Other fixed parameters are also listed in Table 2 for reference. It was worth noting that *Z*-offset calibration was automatically calibrated and was not the focus of this study. Regardless of varied layer thicknesses, total number of layers was 16. To further determine the effects of those key process parameters, the fracture surfaces and internal structures of the samples were observed via conducting an SEM analysis using a scanning electron microscope (SEM) JEOL JSM-6510.

Utilising the Taguchi array yielded a total of 27 distinct combinations of the five key FFF printing process parameters. Each of these combinations, referred to as a "run", encapsulated a unique configuration of extrusion temperature, infill density, layer thickness, printing speed, and number of contours. Within each run, a batch was composed of five identical samples (Fig. 2a) which were subsequently used for tensile testing purposes. The mechanical testing process was conducted using a 5-kN
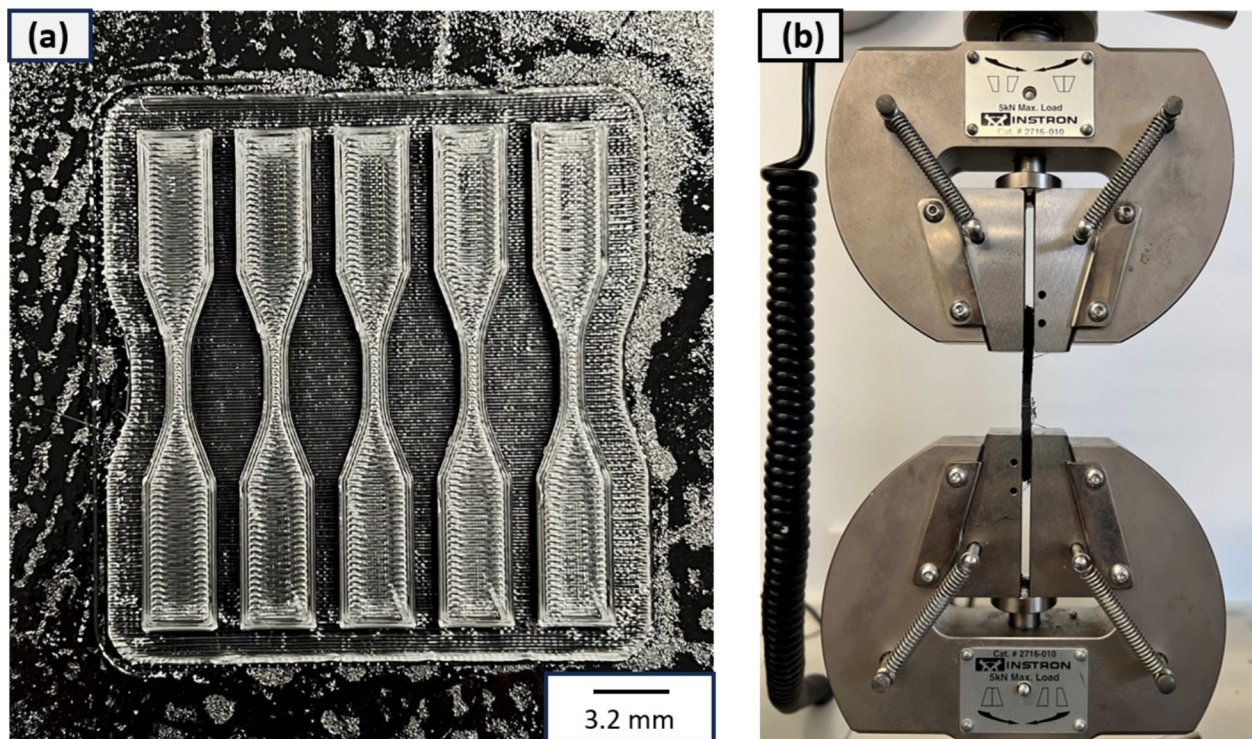
Fig. 2 **a** A batch of testing samples for run 21 and **b** tensile test setup

Instron Machine – Instron 3365 with a strain rate of 1 mm/min (Fig. 2b). The values presented in Table 3 for tensile strength (TS) in each run represent the average across all samples. Likewise, the build time (BT) listed in Table 3 for each run corresponds to the build time required for manufacturing a single sample. Since Taguchi array is an experimental method, build time could be measured by clock physically [33]. However, prior tests demonstrated insignificant difference between computed and actual build time; the build time from the slicer was recorded to reduce the cost of experiment, aiming to automate the optimisation process.

To develop the RSM and ANN models, a total of 27 data in Table 3 were used as training set. Table 4 presents the test set experiments, which were designed to assess the ANN models' effectiveness in response to changes in three critical process parameters: layer thickness, number of contours, and infill density, yielding a dataset of 30 points.

Table 3 Training set

Run	ET	LT	PS	NC	ID	Tensile strength (MPa)	Build time (mins)
1	234	0.1	40	1	40	11.4 ± 1.92	16.0
2	234	0.1	40	1	70	17.1 ± 0.98	21.8
3	234	0.1	40	1	100	33.8 ± 0.87	27.7
4	234	0.2	70	2	40	17.5 ± 0.66	9.0
5	234	0.2	70	2	70	21.0 ± 1.04	11.5
6	234	0.2	70	2	100	33.3 ± 1.44	13.8
7	234	0.3	100	3	40	21.9 ± 1.14	7.2
8	234	0.3	100	3	70	27.0 ± 0.58	8.7
9	234	0.3	100	3	100	33.7 ± 0.54	10.2
10	237	0.1	70	3	40	23.0 ± 2.74	16.8
11	237	0.1	70	3	70	30.5 ± 1.08	20.8
12	237	0.1	70	3	100	35.7 ± 0.79	25.0
13	237	0.2	100	1	40	13.2 ± 1.46	8.2
14	237	0.2	100	1	70	17.9 ± 0.45	10.8
15	237	0.2	100	1	100	33.7 ± 0.47	13.5
16	237	0.3	40	2	40	15.5 ± 1.35	7.8
17	237	0.3	40	2	70	20.2 ± 1.28	9.8
18	237	0.3	40	2	100	32.5 ± 0.76	11.7
19	240	0.1	100	2	40	18.6 ± 0.97	15.2
20	240	0.1	100	2	70	24.3 ± 1.09	19.7
21	240	0.1	100	2	100	36.2 ± 0.79	24.2
22	240	0.2	40	3	40	25.2 ± 0.77	11.5
23	240	0.2	40	3	70	26.7 ± 0.74	13.7
24	240	0.2	40	3	100	34.6 ± 0.87	16.2
25	240	0.3	70	1	40	13.5 ± 1.99	6.3
26	240	0.3	70	1	70	20.2 ± 0.35	8.2
27	240	0.3	70	1	100	32.5 ± 0.48	10.2

Table 4 Test set

Run	ET	LT	PS	NC	ID	Tensile strength (MPa)	Build time (mins)
28	240	0.12	100	1	50	14.5 ± 0.28	13.7
29	240	0.22	100	2	70	23.9 ± 0.81	10.5
30	240	0.28	100	3	90	32.5 ± 0.86	9.7

2.3 Mathematical models

2.3.1 Response surface methodology model

The RSM model is a statistical technique used to approximate and optimise complex relationships between input variables and responses of interest in various experimental settings. The relationships between the output variable Y and the set of key FFF printing process parameters $X_1, X_2, X_3, X_4,$ and X_5 can be captured through Eq. (1). Equation (2) shows a regression model based on the relationship of input and output parameters.

$$Y = f(X_1, X_2, X_3, X_4, X_5) \tag{1}$$

$$Y = K_0 + \sum_{i=1}^{n} K_i X_i + \sum_{i<j}^{n} K_{ij} X_i X_j + \sum_{i=1}^{n} K_{ii} X_i^2 + \varepsilon \tag{2}$$

Based on the standard regression equation, the mathematical model for selected parameters can be represented as Eq. (3).

$$\begin{aligned} Y = {} & K_0 + K_1 ET + K_2 LT + K_3 PS + K_4 NC + K_5 ID \\ & + K_{12} ET * LT + K_{13} ET * PS + K_{14} ET * NC \\ & + K_{15} ET * ID + K_{23} LT * PS + K_{24} LT * NC \\ & + K_{25} LT * ID + K_{34} PS * NC + K_{35} PS * ID \\ & + K_{45} NC * ID + K_{11} ET^2 + K_{22} LT^2 + K_{33} PS^2 \\ & + K_{44} NC^2 + K_{55} ID^2 \end{aligned} \tag{3}$$

where, Y is the response corresponding to the selected process parameters; $K_0, K_i, K_{ii},$ and K_{ij} are constant, linear, square, and interaction coefficients, respectively; $X_1, X_2, X_3, X_4,$ and X_5 are the input parameters; ε is the residual error.

After eliminating the irrelevant terms, the final mathematical models were loaded as fitness functions into the multi-objective GA.

2.3.2 Artificial neural network model

Addressing the existing research gap, this study explores the effectiveness of a recently introduced neural network regression model, fitrnet, available in MATLAB 2022®. A distinctive feature of this model lies in its capacity to autonomously optimise an extensive spectrum of hyperparameters, encompassing variables such as the number of hidden layers, neurons, activation functions, and the regularisation parameter lambda. To determine the optimal architecture, the search was extended up to a maximum of five hidden layers and 400 neurons, accompanied by an assessment of three commonly employed transfer functions: relu, sigmoid, and tanh. Because the cross-validation was adopted, the dataset was split with a 90:10 ratio, resulting in 27 data points for training and 3 for testing. Recognising the extensive search domain, the limited-memory Broyden–Fletcher–Goldfarb–Shanno algorithm (LBFGS) and Bayesian optimisation approach were harnessed to streamline computational efficiency.

Throughout the training process, the Bayesian optimisation method orchestrated a reduction in cross-validation loss, depicted as a function $m(x)$ in Eq. (5) which involves mean squared error (MSE) loss function computed in Eq. (4), culminating in the determination of the optimal set of hyperparameters upon reaching the maximal objective evaluations [34, 35].

$$MSE = \frac{1}{N} \sum_{i=1}^{N} \left(Y_i - \widehat{Y}_i \right)^2 \tag{4}$$

$$m(x) = \ln(1 + loss) = \ln(1 + MSE) \tag{5}$$

Notably, it was observed that the optimal architectural configuration did not invariably align with the final objective evaluation. Further insights into the hyperparameters optimisation process can be found in Table 5.

Table 5 Hyperparameter optimisation

Type of network	Feedforward network
Optimisation method	Bayesian optimisation
Solver	Limited-memory Broyden–Fletcher–Goldfarb–Shanno algorithm (LBFGS)
Activations	Relu, Sigmoid, Tanh
Number of hidden layers range	(1, 5)
Number of hidden neurons range	(1, 400)
Regularisation parameter lambda range	(2.4e-7, 2.4e + 3)
Maximum objective evaluations	60
K-fold cross-validation	10
Data division	Train set: 90%, test set 10%

Figure 3 shows the ANN architecture used in the current study with five inputs as extrusion temperature, layer thickness, printing speed, number of contours, and infill density and one single response as a separate model was built for both tensile strength and build time. For fastening the training process, all the inputs were normalised to $(-1, 1)$ using Eq. (6) where $X_n, X_r, X_{r\min}$, and $X_{r\max}$ are the normalised, raw, minimum, and maximum values of input parameters, respectively [6].

$$X_n = 2\frac{X_r - X_{r\min}}{X_{r\max} - X_{r\min}} - 1 \qquad (6)$$

2.4 Optimisation

2.4.1 Multi-objective genetic algorithm

The optimisation of process parameters is of paramount importance in ensuring the desirable performance of a given system. However, it is worth noting that achieving the optimal condition for a specific response variable may not necessarily align with the optimal settings for other response variables, potentially leading to conflicting objectives. This intricacy underscores the necessity for multi-objective optimisation strategies, which seek to strike a harmonious balance between diverse and often conflicting objectives. In this work, the RSM and ANN models were incorporated with the multi-objective genetic algorithm (GA) to seek the optimal conditions, aiming to optimise both the tensile strength and build time. The tensile strength was subjected to maximise while minimising the build time. GA originated from John Holland's work in the 1960s and was inspired by the process of natural evolution. GA involves creating a population of potential solutions, selecting the best-performing individuals, applying genetic operations like crossover and mutation to create new solutions, and repeating this process iteratively to evolve towards optimal solutions for complex optimisation problems [36].

2.4.2 TOPSIS method

In this study, TOPSIS was adopted to determine the best optimal parameters from sets of solutions provided by RSM-GA and ANN-GA. TOPSIS plays a pivotal role in multi-objective optimization by systematically ranking alternatives based on their closeness to both the ideal and anti-ideal solutions, aiding in informed decision-making. The main steps of TOPSIS involve constructing a normalised decision matrix from the original data, calculating the weighted normalised decision matrix by assigning appropriate weights to each criterion, determining the ideal and anti-ideal solutions, and then calculating the distances of each alternative from these solutions. Finally, a preference index is obtained by comparing the distances and ranking the alternatives to guide decision-making in multi-criteria scenarios [37].
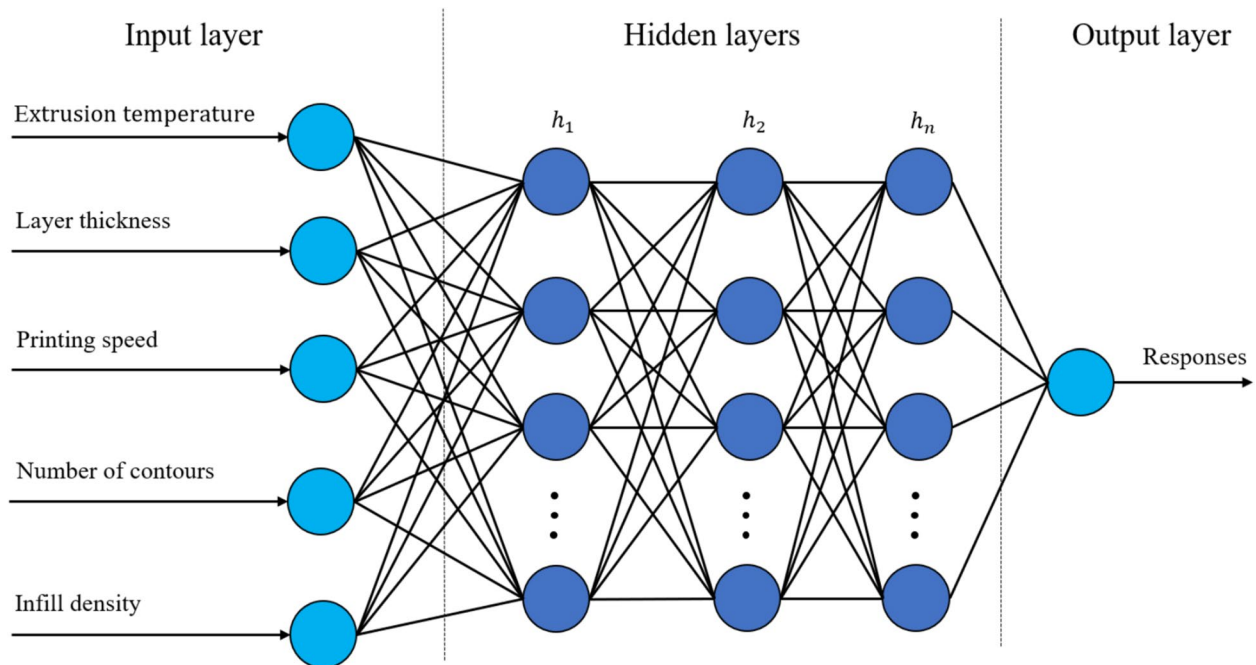

Fig. 3 ANN model with five inputs and one output

3 Results and discussion

3.1 RSM models

The RSM models for tensile strength and build time are shown in Eqs. (7) and (8). The statistical significance of the process parameters is evaluated using p and f values of ANOVA. The fitted model should have $p < 0.05$. Coefficient of determination R^2 defines the fitness of data with the regression line. The higher value of R^2 signifies the good fit of model.

$$TS = 1349 - 11.9\,ET - 0.6\,LT + 0.104\,PS + 6.10\,NC + 0.84\,ID$$
$$+ 0.0263\,ET * ET + 7.3\,LT * LT + -0.000659\,PS * PS + 0.745\,NC * NC$$
$$+ 0.003459\,ID * ID - 0.00369\,ET * ID - 0.139\,LT * ID$$
$$+ 0.000085\,PS * ID - 0.0781\,NC * ID \tag{7}$$

$$BT = 632 - 5.3\,ET - 137.18\,LT - 0.1055\,PS - 0.250\,NC + 0.684\,ID$$
$$+ 0.0113\,ET * ET + 282.4\,LT * LT + 0.000638\,PS * PS + 0.407\,NC * NC$$
$$+ 0.000021\,ID * ID - 0.00185\,ET * ID - 0.5046\,LT * ID$$
$$- 0.000262\,PS * ID - 0.01389\,NC * ID \tag{8}$$

Table 6 displays the ANOVA findings concerning the prediction of the tensile strength. The mathematical model demonstrates a satisfactory predictive capacity, yielding a R^2 value of 98.02%. The contribution of each factor was calculated as its sequential sum of squares (Seq SS) divided by the total sequential sum of squares (SST), expressed as a percentage. In terms of contribution percentages, infill density (ID) emerges as the foremost influential factor, accounting for 73.66% of the variation, followed by the number of contours (NC) contributing 14.58%. Moreover, the number of contours (NC) maintains statistical significance with a p-value below 0.05. Additionally, both the terms ID*ID and NC*ID exhibit notable statistical significance.

Table 7 presents the ANOVA findings pertaining to the prediction of the build time. The mathematical model exhibits a commendable predictive capability, culminating in a R^2 value of 99.63%. In the context of contribution percentages, layer thickness (LT) takes centre stage as the most influential factor, encompassing 70.17% of the variability, trailed by infill density (ID) contributing 18.04%. Furthermore, layer thickness (LT) preserves its statistical significance with a p-value below 0.05. Additionally, noteworthy statistical significance is observed in the terms PS, LT*LT, PS*PS, LT*ID, and NC*ID.

A recommended practice for evaluating the goodness of fit of a model is to apply the Anderson–Darling test to the residuals. This test assesses the extent to which data points deviate from the fitted line on a probability plot. If the p-value from the Anderson–Darling test is lower than the chosen significance level (e.g. 0.05 or 0.10), it suggests that the data do not follow a normal distribution. Figure 4a and b show the normal probability plots of residuals, both of which exhibit p-values greater than the significance level

Source	DF	Seq SS	Contribution	Adj SS	Adj MS	F-value	P-value
Regression	14	1586.19	98.20%	1586.19	113.299	46.79	0.000
ET	1	12.75	0.79%	0.31	0.307	0.13	0.728
LT	1	9.94	0.62%	0.00	0.001	0.00	0.983
PS	1	4.97	0.31%	2.35	2.348	0.97	0.344
NC	1	235.52	14.58%	11.73	11.727	4.84	0.048
ID	1	1189.73	73.66%	1.21	1.211	0.50	0.493
ET*ET	1	0.34	0.02%	0.34	0.335	0.14	0.716
LT*LT	1	0.03	0.00%	0.03	0.032	0.01	0.911
PS*PS	1	2.11	0.13%	2.11	2.113	0.87	0.369
NC*NC	1	3.33	0.21%	3.33	3.330	1.38	0.264
ID*ID	1	58.14	3.60%	58.14	58.143	24.01	0.000
ET*ID	1	1.33	0.08%	1.33	1.327	0.55	0.473
LT*ID	1	2.10	0.13%	2.10	2.095	0.87	0.371
PS*ID	1	0.07	0.00%	0.07	0.069	0.03	0.868
NC*ID	1	65.83	4.08%	65.83	65.834	27.19	0.000
Error	12	29.06	1.80%	29.06	2.421		
Total	26	1615.25	100.00%				
Std	1.56						
R^2	98.20%						
R^2(adj)	96.10%						
R^2(pred)	91.21%						

Table 6 Variance for tensile strength

Table 7 Variance for build time

Source	DF	Seq SS	Contribution	Adj SS	Adj MS	*F*-value	*P*-value
Regression	14	905.907	99.63%	905.907	64.7076	233.20	0.000
ET	1	0.039	0.00%	0.060	0.0596	0.21	0.651
LT	1	638.039	70.17%	59.250	59.2496	213.53	0.000
PS	1	19.358	2.13%	2.420	2.4205	8.72	0.012
NC	1	2.988	0.33%	0.020	0.0197	0.07	0.795
ID	1	164.006	18.04%	0.801	0.8015	2.89	0.115
ET*ET	1	0.062	0.01%	0.062	0.0622	0.22	0.644
LT*LT	1	47.852	5.26%	47.852	47.8524	172.45	0.000
PS*PS	1	1.977	0.22%	1.977	1.9774	7.13	0.020
NC*NC	1	0.996	0.11%	0.996	0.9959	3.59	0.083
ID*ID	1	0.002	0.00%	0.002	0.0021	0.01	0.933
ET*ID	1	0.333	0.04%	0.333	0.3333	1.20	0.295
LT*ID	1	27.502	3.02%	27.502	27.5023	99.12	0.000
PS*ID	1	0.669	0.07%	0.669	0.6690	2.41	0.146
NC*ID	1	2.083	0.23%	2.083	2.0833	7.51	0.018
Error	12	3.330	0.37%	3.330	0.2775		
Total	26	909.237	100.00%				
Std	0.53						
R^2	99.63%						
R^2(adj)	99.21%						
R^2(pred)	97.06%						

of 0.05. Therefore, the experimental residuals demonstrate good fit, and it is reasonable to assume that they exhibit a normal distribution.

3.2 Effect of 3D printing process parameters on selected responses

The experimental results show the significant impact of those five key FFF printing process parameters on selected responses. The main effects plot for tensile strength are presented in Fig. 5.

The most vivid characteristic is the rapid increase in tensile strength when the infill density changes from 40 to 100%. Indeed, increasing infill density creates a denser internal structure with enhanced material bonding, reducing voids and defects, and increasing stiffness, all of which collectively contribute to better load distribution and resistance to applied forces. In their study, Tura, Lemu [20], also discovered that a 100% infill density maximises tensile strength when investigating the combined impact of infill density, extrusion temperature, and printing speed. In another investigation [38], the influence of infill density across a range of 20 to 100%, alongside variables like layer thickness, extrusion temperature, and infill pattern, were explored and a consistent upward trend in tensile strength was found with the highest point observed at an infill density of 100%. As the contour consists of deposited filament aligned with the applied load, increasing number of contours can lead to the enhancement in tensile properties [13], which are evident in Fig. 5. This finding aligns with the research findings by Singh, Singh [39], which identified the highest tensile strength at 3 contours, the optimal level while exploring the impact of raster angle, number of contours, layer thickness, infill density, and solid layers on FFF printed dog-bone tensile strength. Additionally, another literature supported this trend by demonstrating the consistent enhancement of dynamic modulus with an increase in the number of contours [40]. As depicted in Fig. 5, a trend emerges where lower layer thickness corresponds to improved strength. This finding is supported by numerous research as decreasing the layer thickness promotes finer inter-layer bonding, minimising the risk of delamination and surface defects, resulting in a more cohesive and uniform structure that can better withstand applied forces [12, 28, 39, 41]. Apart from strongly enhancing tensile strength, lower layer thickness was also agreed to reduce the surface roughness [8, 26, 42] and improve dimensional accuracy [43, 44]. Although those studies highlighted that the increase of layer thickness could negatively affect the tensile strength, this study shows that its effect is not significant compared to the number of contours and infill density. Furthermore, increasing the printing speed and extrusion temperature within the defined range is observed to enhance tensile properties, indicating the viability of employing higher printing speeds to decrease build time without compromising strength.

Fig. 4 Anderson–Darling normality test: (**a**) residuals TS and (**b**) residuals BT
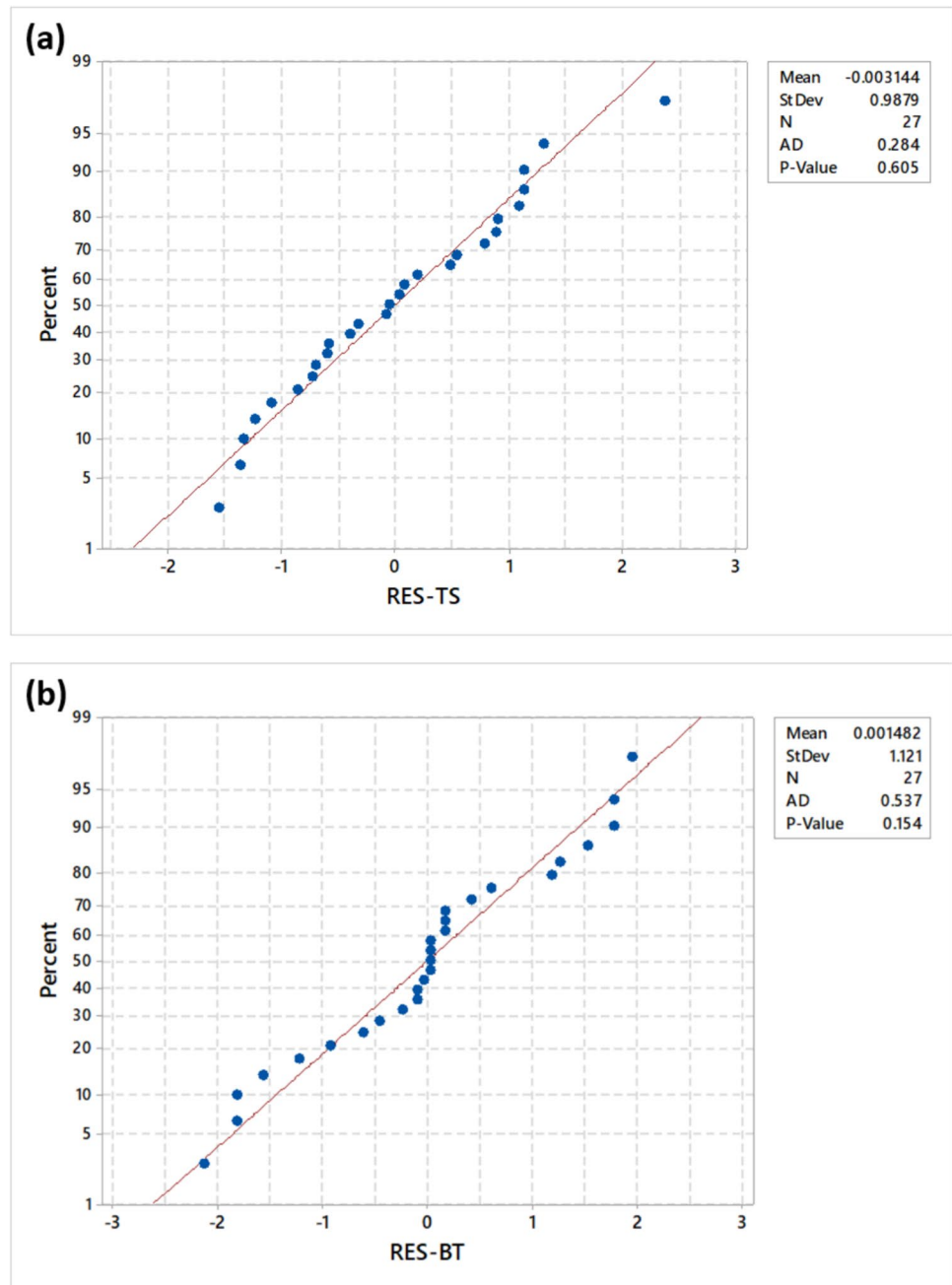
The interactive impacts of the studied parameters on build time are illustrated in Fig. 6. This aligns with those findings in Table 7, where transitioning layer thickness from 0.1 to 0.3 mm correlates with a notable reduction in build time. Kumar, Gupta [6], similarly identified the noteworthy influence of layer thickness while pursuing optimisation of build time and surface roughness. In a separate investigation, layer thickness emerged as the most influential factor with a contribution of 84.6%, highlighting its significance in achieving reduced build time, particularly at lower layer thickness levels [45].

On the other hand, increasing infill density results in a more compact structure, consequently elongating the printing duration, as evidenced by an upward trend of build time when the infill density varied from 40 to 100%. Intuitively, elevating the printing speed should logically reduce the printing duration, as agreed by Kumar et al. [6]. Nevertheless, no considerable distinction is noted when the printing speed is adjusted between 70 and 100 mm/s. Notably, while the number of contours plays a pivotal role in enhancing tensile strength, its influence on build time remains relatively insignificant. Hence, when the printing geometry and

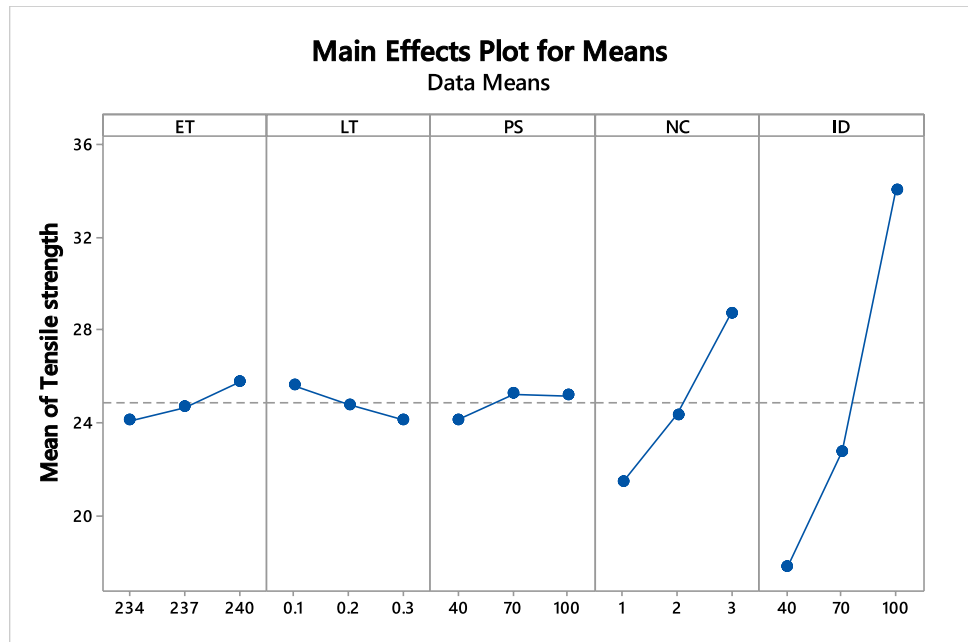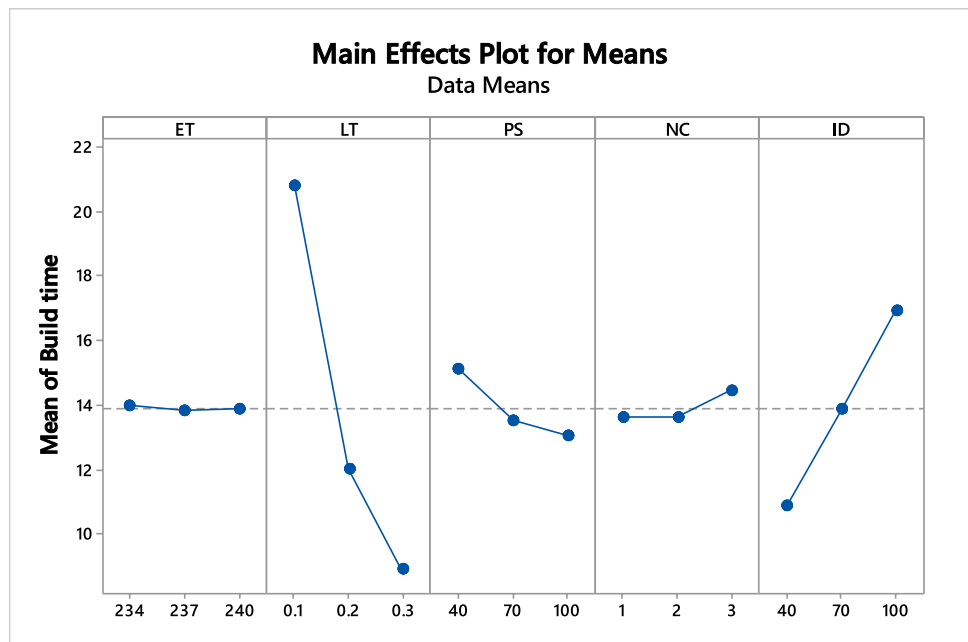**Fig. 5** Main effect plots for tensile strength

Fig. 6 Main effect plots for build time

conditions permit a substantial number of contours, printing the parts with a reasonable number of contours can boost the strength without compromising on the build time.
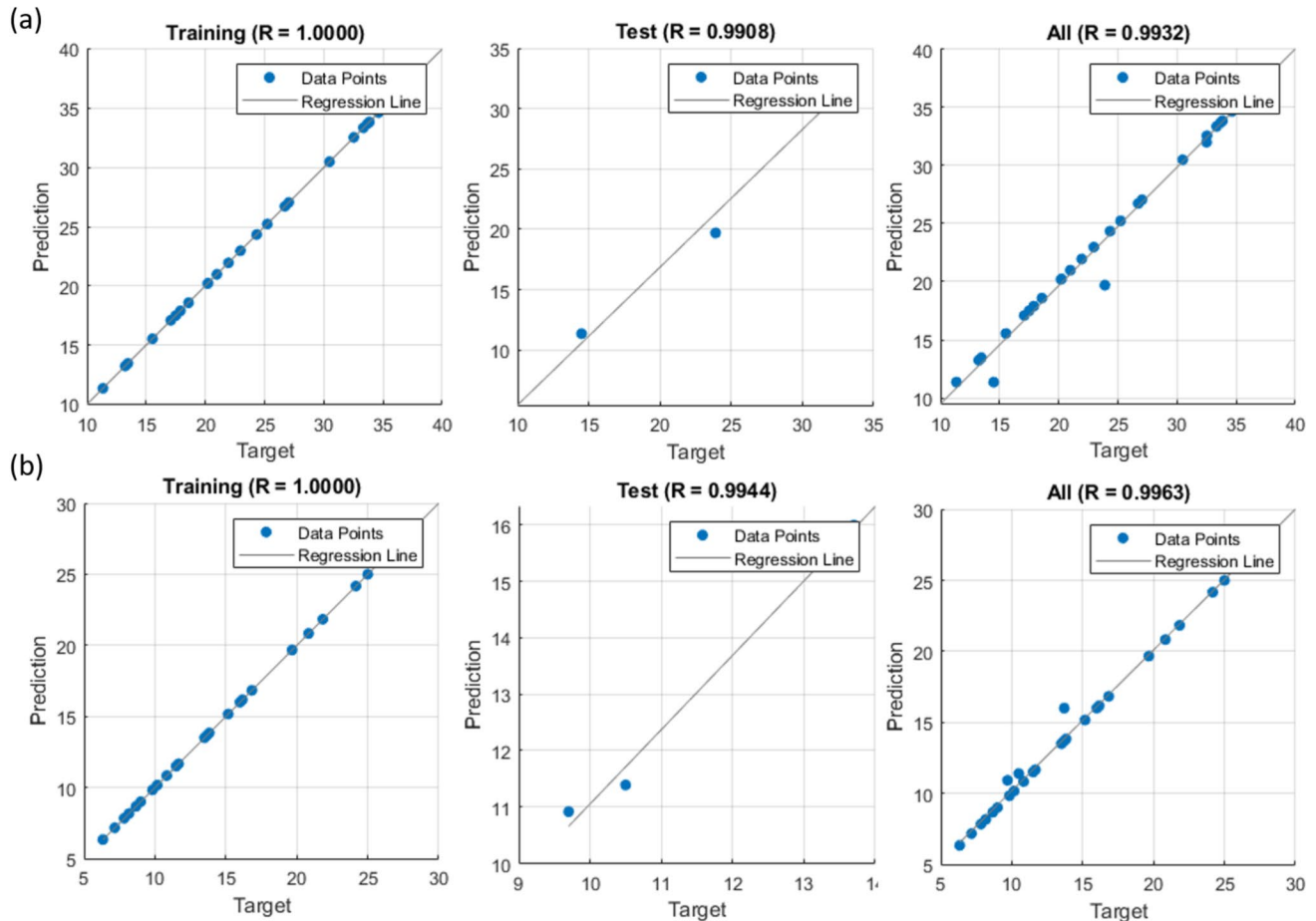
3.3 ANN models

Upon conducting 60 evaluations, the architectural optimisation for ANN models concluded, encompassing all hyperparameters outlined in Table 8. Interestingly, the predictive model for tensile strength necessitates only one layer and 34 neurons, whereas the build time model necessitates four

layers. Evidently, executing this process using a standard manual approach proves impractical due to the requirement for up to 372 maximum hidden neurons. As observed in Fig. 7, the optimisation process was notably successful, as evidenced by the correlation coefficient Rs for both the ANN models to predict the tensile strength and build time. This finding further confirms the effectiveness of our method developed to construct the ANN discussed in the previous study [46]. It was noted that for the test set, with a maximum error of merely 4.51%, the ANN models proved adequately effective in aiding designers to strike a balance between

Table 8 Optimal ANN architecture

Response	Number of hidden layers	Activations	Lambda	Number of neurons in each hidden layer			
				Layer 1	Layer 2	Layer 3	Layer 4
Tensile strength	1	Sigmoid	7.40e-5	34	-	-	-
Build time	4	Sigmoid	5.62e-7	49	5	181	372

Fig. 7 Regression plots corresponding to optimal training algorithm for (**a**) tensile strength and (**b**) build time

diverse parameters while maintaining desired levels of tensile strength and build time. In addition, the developed ANN model has proved capable of forecasting the tensile strength and build time at various combination of process parameters. Therefore, this model can be adopted in practical where several applications opt for reduced layer thickness and infill density to optimise material usage or when the part geometry limits the number of contours.

The findings of this section underscore why the limited exploration of up to three hidden layers and a constrained neuron count led to the failure of ANN to effectively capture the surface roughness pattern amid variations in layer thickness, infill density, printing speed, and extrusion

temperature, resulting in notably low accuracy [17]. To transcend the trial-and-error limitations of initialising ANN models, Meiabadi, Moradi [47], employed a novel approach by integrating a genetic algorithm (GA) to optimise the performance of ANN. Additionally, in another literature, the shortcomings of manual calibration were mitigated by amalgamating the outputs of all 36 models to yield superior performance compared to relying on a single network [19]. Nonetheless, these aforementioned approaches appear intricate and time-consuming in contrast to the current study's proposed method, which conveniently automates architecture optimisation, a boon for researchers less acquainted with the intricacies of ANN.

4 Optimisation and validation

The chosen objectives inherently oppose one another, requiring the maximisation of tensile strength while concurrently minimising build time. To address this dilemma, a multi-objective genetic algorithm in MATLAB 2022® was applied to optimise both RSM and ANN models, effectively identifying a comprehensive range of optimised parameter sets. The constraints for all models are $234 \leq ET \leq 240, 0.1 \leq LT \leq 0.3, 40 \leq PS \leq 100, 1 \leq NC \leq 3$, and $40 \leq ID \leq 100$. To address the multi-objective nature of the problem, specialised techniques were employed to compare and rank individuals based on their performance across different objectives. These techniques help identify a set of solutions known as Pareto optimal solutions. The Pareto front represents the trade-offs between the objectives, where improving one objective may lead to a degradation in another. After acquiring the list of optimal solutions ranked by TOPSIS, it was observed that the numerical values of top solutions were closely clustered and not practically achievable for the 3D printer. Consequently, for each solution, the numerical values of extrusion temperature and number of

contours were approximated to the nearest integer; the printing speed and infill density were rounded to the nearest ten; and the layer thickness values were rounded to the nearest two decimal points. For example, if the original TOPSIS solutions resulted in 235.5°C ET, 0.206 mm LT, 85 mm/s PS, 2.5 NC, and 98% ID, the adjusted solutions would be 236°C ET, 0.21 mm LT, 90 mm/s PS, 3 NC, and 100% ID. Subsequently, an additional step was executed to eradicate identical solutions before feeding the inputs into the RSM and ANN models for generating new predictive tensile strength and build time. In the end, TOPSIS was carried out again to rank the solutions using appropriate weights for the two responses. With this procedure, the adjusted TOPSIS tables covered a wider range of possible solutions for optimisation.

The optimal solutions for every RSM model are presented in Table 9. The RSM-GA-TOPSIS provided optimum tensile strength, and build time of 41.5 MPa, and 0.2 min, respectively, corresponding to 240°C ET, 0.21 mm LT, 90 mm/s PS, 3 NC, and 100% ID.

Table 10 lists the set of optimal solutions for every ANN model. The ANN-GA-TOPSIS method resulted in 36.6 MPa

Table 9 Suggested optimal solutions by GA for RSM models

Sol No.	ET	LT	PS	NC	ID	Tensile strength (MPa)	Build time (mins)	Ranking
1	240	0.21	90	3	100	41.5	0.2	1
2	240	0.20	90	3	100	41.7	0.9	2
3	240	0.19	90	3	100	41.8	1.7	3
4	240	0.18	90	3	100	41.9	2.5	4
5	240	0.17	90	3	100	42.0	3.4	5
6	240	0.16	90	3	100	42.1	4.4	6
7	240	0.15	90	3	100	42.3	5.4	7
8	240	0.14	90	3	100	42.4	6.4	8
9	240	0.13	90	3	100	42.5	7.5	9
10	240	0.12	90	3	100	42.6	8.7	10

Table 10 Suggested optimal solutions by GA for ANN models

Sol No.	ET	LT	PS	NC	ID	Tensile strength (MPa)	Build time (mins)	Ranking
1	240	0.30	100	3	100	36.6	10.1	1
2	239	0.30	100	3	100	36.4	10.2	2
3	240	0.29	100	3	100	36.6	10.4	3
4	240	0.28	100	3	100	36.7	10.9	4
5	240	0.30	100	2	100	35.7	9.8	5
6	240	0.27	100	3	100	36.7	11.5	6
7	239	0.30	100	2	100	35.5	9.8	7
8	240	0.25	100	3	100	36.8	12.0	8
9	240	0.26	100	3	100	36.8	12.1	9
10	240	0.22	100	3	100	36.9	13.6	10

tensile strength, and 10.1 min build time corresponding to 240°C ET, 0.3 mm LT, 100 mm/s PS, 3 NC, and 100% ID. In an overview, the proposed methodologies led to enhancement in response parameters.

Validation experiments were carried out to ensure the reliability of the proposed methodologies. For each of the RSM-GA-TOPSIS and ANN-GA-TOPSIS methods, the first-rank solution was selected for part fabrication. Standard specimens were subsequently manufactured and subjected to mechanical property testing and build time records.

Table 11 presents the comparative results and percentage improvement in response corresponding to different methods.

It is worth noting that "predicted responses" only represent the values generated by the RSM and ANN models after inputting the optimal solutions. Therefore, experiments were carried out to collect data for "experimental response". The purposes were to evaluate the efficiency of the predictive models and provide the actual tensile strength generated by the optimal solutions. For the ASTM test, the maximum tensile strength (MaxTS) was found at run 21 with 36.2 MPa and the time for fabricating one sample is 24.2 min. The experimental tensile strength achieved through the RSM-GA method is 36.0 MPa, requiring 12.8 min for printing. While the tensile strength decreases by 0.6%, the build time shows an improvement of 47%. Notably, substantial discrepancies exist between predicted and experimental values for RSM-GA, with deviations of 15.2% for tensile strength and 98% for build time. On the other hand, through the ANN-GA method, the experimental tensile strength reached 34.6 MPa, with a printing time of 10.2 min. When comparing to MaxTS, despite a 4.4% decrease in tensile strength, the build time of ANN-GA demonstrated a superior enhancement of 58%, which is 11% higher than the 47% enhancement achieved by RSM-GA. Significantly, in evaluating predictive model efficacy, ANN-GA outperformed RSM-GA, exhibiting a mere 5.7% error in predicting tensile strength

and a minimal 0.7% error in forecasting build time. Within this context, ANN-GA emerges as a more fitting model for comprehending the non-linear impact of key FFF printing process parameters and facilitating optimisation. A trade-off of 4.4% in the tensile strength in exchange for a 58% reduction in the build time is deemed acceptable.

## 5 SEM analysis on fractography

As ANN-GA model yielded better prediction accuracy, the SEM images of the ANN-GA were captured to compared with the MaxTS. In addition, SEM images of run 28, run 29, and run 30 were also observed for demonstrating the effects of key FFF printing process parameters on internal structures of the specimens. Figure 8 presents the SEM images of MaxTS, ANN-GA, run 28, run 29, and run 30 captured at ×25 and ×100 magnifications, where yellow circles demonstrate air voids inside the structure and blue rectangles indicate contour regions.

From the SEM images, there are two types of air voids observed in the internal structures. The first type is caused by the essence of infill density while the second one is induced by the intrinsic elements [30]. At a lower LT of 0.1 mm, the MaxTS (Fig. 8a and b) illustrates less air voids then ANN-GA (Fig. 8c and d) printed at 0.3-mm LT, confirming the higher TS observed for MaxTS. Denser structures such as Max TS (Fig. 8a and b) and ANN-GA (Fig. 8c and d) were affirmed to yield a better strength based on the current literature [10, 12]. However, in term of part quality, MaxTS demonstrates a slight over-extrusion and warping. That was due to the effect of Z-offset of the nozzle. Although the Z-offset calibration was often carried out automatically by the printer, manual optimisation could further improve the part quality [48]. Therefore, the optimal set ANN-GA not only reduces the build time significantly but also improves the part quality despite of the 4.4% reduction in the TS. On

Table 11 Process parameters and their levels

Particular	Parameter	MaxTS	RSM-GA	ANN-GA
Optimised parameters	ET (°C)	240	240	240
	LT (mm)	0.10	0.21	0.30
	PS (mm/s)	100	90	100
	NC	2	3	3
	ID (%)	100	100	100
Predicted response	TS (MPa)	-	41.5	36.6
	BT (mins)	-	0.2	10.1
Experiment responses	TS (MPa)	36.2 ± 0.79	36.0 ± 0.53	34.6 ± 0.51
	BT (mins)	24.2	12.8	10.2
Errors (%)	TS (MPa)	-	15.2	5.7
	BT (mins)	-	98.0	0.7
Improvement in TS, BT			$-0.6\%, 47\%$	$-4.4\%, 58\%$

Fig. 8 SEM images of MaxTS at ×25 (**a**) and ×100 (**b**); ANN-GA at ×25 (**c**) and ×100 (**d**); run 28 at ×25 (**e**) and ×100 (**f**); run 29 at ×25 (**g**) and ×100 (**h**); and run 30 at ×25 (**i**) and ×100 (**j**) magnifications (notes: Yellow circles show the air voids presented in the samples. Blue rectangles show contour regions)
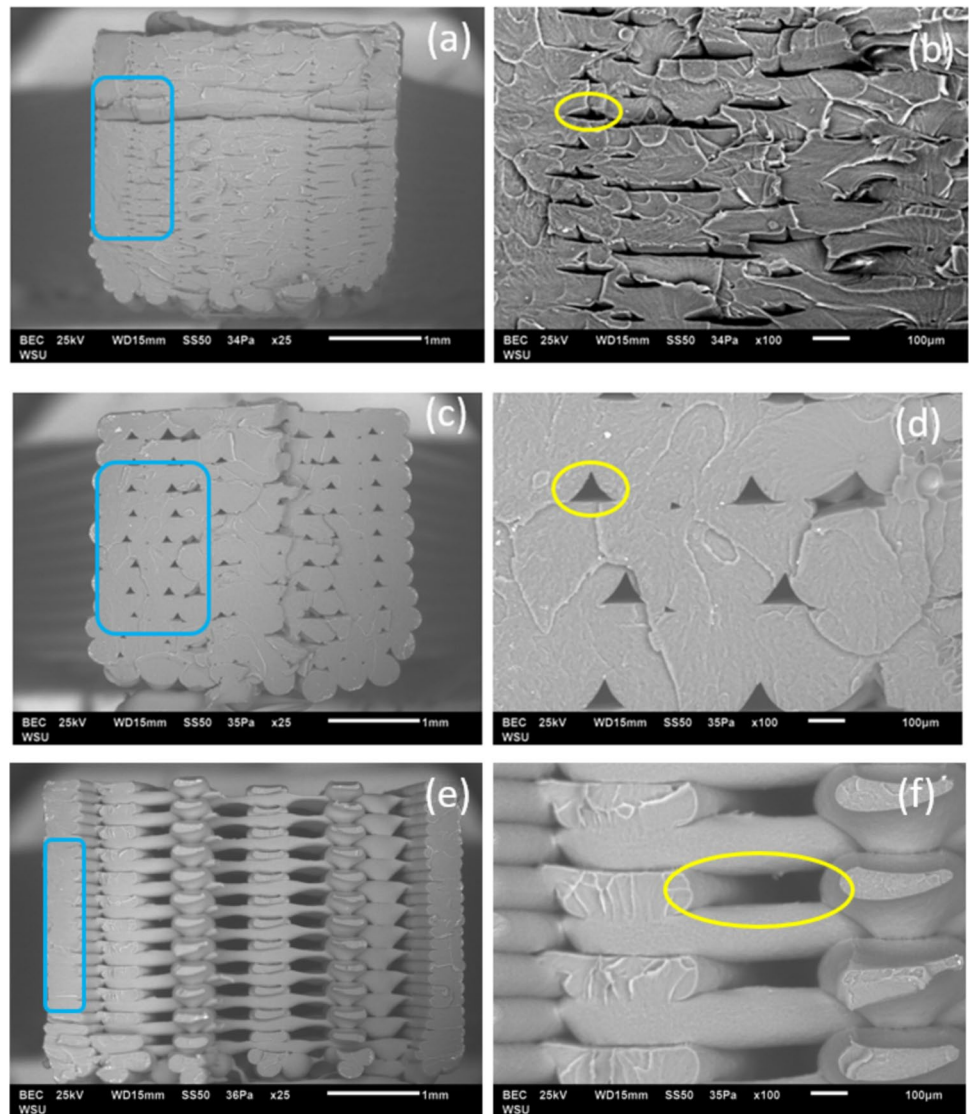
the other hand, the SEM images of run 28, run 29, and run 30 clearly indicates the change of internal structures at various infill density, layer thickness, and number of contours. It is observed that higher LT leads to higher height and width ratios of the intrinsic elements, generating larger air voids between the elements. Meanwhile, the increase of contours does not affect the general quality of the internal structures and thus can be adopted to strengthen the printed product without compromising the build time.

6 Conclusions

This study develops a systematic experimental and theoretical analysis and optimisation framework to optimise the FFF printing process for thermoplastics with adopting statistical methods and multi-criteria decision-making and using ABS as the exemplar. The validated model parameters were

verified through experiments involving standard specimens and actual applications. The discussion of results yields subsequent conclusions as follows.

- The significant improvement in tensile strength occurs by increasing ET (234 to 240°C), NC (1 to 3), ID (40 to 100%), and decreasing LT (from 0.3 to 0.1 mm). The maximum experimental value tensile strength (36.2 MPa) was attained at run 21 with 240°C ET, 0.1 mm LT, 100 mm/s PS, 2 NC, and 100% ID. However, the build time was compromised at these corresponding values.
- According to the percentage of contribution analysis, infill density emerged as the most influential factor affecting tensile strength with 73.7% of contribution, followed by the number of contours with 14.6% of contribution. In contrast, build time was predominantly influenced by layer thickness with 70.2% of contribution, trailed by infill density with 18.0% of contribution.

Fig. 8 (continued)
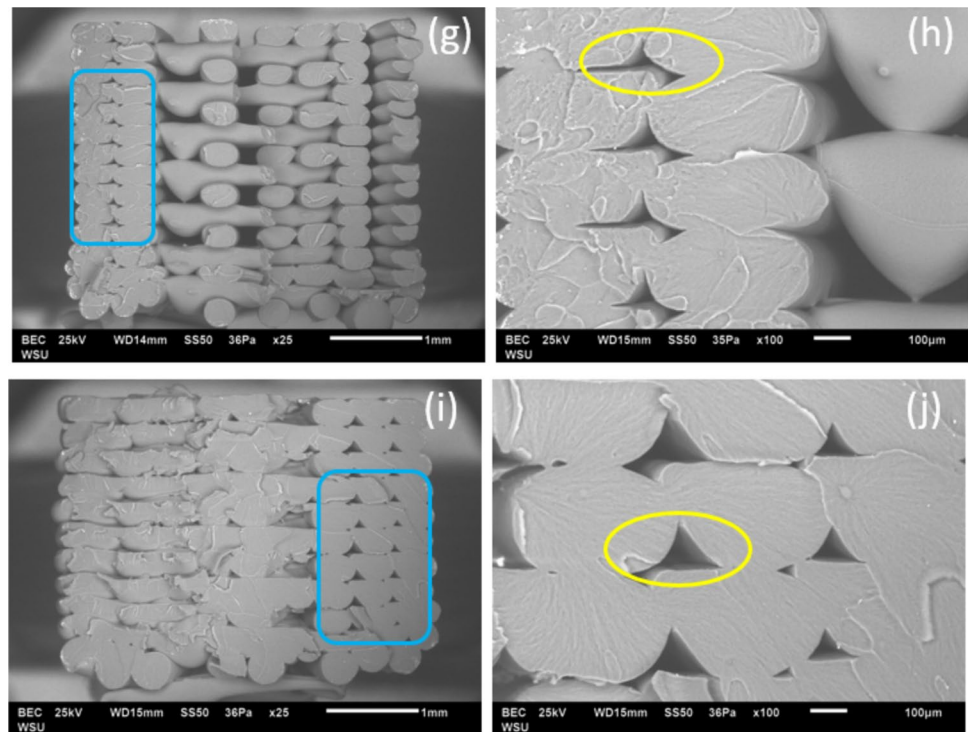
- Although the RSM-GA-TOPSIS resulted in a 0.6% decrease in tensile strength, the build time was improved by 47%, corresponding to 240°C ET, 0.21 mm LT, 90 mm/s PS, 3 NC, and 100% ID. Similarly, ANN-GA-TOPSIS compromised only 4.4% of tensile strength to reduce the build time by 58%, corresponding to 240°C ET, 0.30 mm LT, 100 mm/s PS, 3 NC, and 100% ID.
- Although the RSM-GA-TOPSIS approach demonstrated enhancement in properties, high discrepancies between the predictive and experimental values were recorded, 18% for tensile strength, and 98% for build time. Therefore, this optimisation method is not recommended for future applications as it will produce experimental cost to validate the predictive optimal solutions.
- The ANN-GA-TOPSIS approach demonstrated a superior efficiency in capturing data patterns and conducting optimisation. The proposed methodology for constructing ANN models proved successful, poised to replace the manual approach. Further experimental tests extended the utility of ANN models, facilitating designers in parameter optimisation while upholding both tensile strength and build time requirements.

Multi-objective optimisation methods have been proven much more effective in yielding optimal results compared to single-objective optimization. The findings of this study hold significant implications for designers and manufacturers of domestic and small industrial components, aiding in the comprehensive understanding of how process parameters collectively influence part characteristics. Furthermore, the approach proposed in this study bears relevance for various applications, whether involving diverse materials or response parameters.

Data availability Not applicable.

Code availability Not applicable.

Declarations

Ethics approval Not applicable.

Consent to participate Not applicable.

Consent for publication All authors commented on previous versions of the manuscript. All authors read and approved the final manuscript.

Conflict of interest The authors declare no competing interests.

References

1. Ngo TD et al (2018) Additive manufacturing (3D printing): a review of materials, methods, applications and challenges. Composites Part B-Engineering 143:172–196
2. Wang X et al (2017) 3D printing of polymer matrix composites: a review and prospective. Compos B Eng 110:442–458
3. Mwema FM, Akinlabi ET (2020) Basics of fused deposition modelling (FDM). Fused Deposition Model 30:1–15. https://doi.org/10.1007/978-3-030-48259-6_1
4. Zohdi N, Yang R (2021) Material anisotropy in additively manufactured polymers and polymer composites: a review. Polymers 13(19):3368
5. Abas M et al (2021) Development of prediction model for conductive pattern lines generated through positive displacement microdispensing system using artificial neural network. Arab J Sci Eng 46(3):2429–2442
6. Kumar P, Gupta P, Singh I (2022) Parametric optimization of FDM using the ANN-based whale optimization algorithm. Ai Edam-Artificial Intelligence for Engineering Design Analysis and Manufacturing 36:36
7. Kechagias JD (2024) Surface roughness assessment of ABS and PLA filament 3D printing parts: structural parameters experimentation and semi-empirical modelling. The International Journal of Advanced Manufacturing Technology 134(3–4):1935–1946
8. Cerro A et al (2021) Use of machine learning algorithms for surface roughness prediction of printed parts in polyvinyl butyral via fused deposition modeling. Int J Adv Manuf Technol 115(7–8):2465–2475
9. Mahmood S, Qureshi AJ, Talamona D (2018) Taguchi based process optimization for dimension and tolerance control for fused deposition modelling. Addit Manuf 21:183–190
10. Deshwal S, Kumar A, Chhabra D (2020) Exercising hybrid statistical tools GA-RSM, GA-ANN and GA-ANFIS to optimize FDM process parameters for tensile strength improvement. CIRP J Manuf Sci Technol 31:189–199
11. Tura AD, Lemu HG, Mamo HB (2022) Experimental investigation and prediction of mechanical properties in a fused deposition modeling process. Crystals 12(6):844
12. Wang SH et al (2020) Effects of fused deposition modeling process parameters on tensile, dynamic mechanical properties of 3D printed polylactic acid materials. Polym Testing 86:106483
13. Giri J et al (2021) Optimization of FDM process parameters for dual extruder 3d printer using artificial neural network. Materials Today-Proceedings 43:3242–3249
14. Kechagias JD et al (2024) Experimental investigation and neural network development for modeling tensile properties of polymethyl methacrylate (PMMA) filament material. The International Journal of Advanced Manufacturing Technology 134(9–10):4387–4398
15. Samykano M et al (2019) Mechanical property of FDM printed ABS: influence of printing parameters. Int J Adv Manuf Technol 102(9–12):2779–2796
16. Vijayaraghavan V et al (2015) Process characterisation of 3D-printed FDM components using improved evolutionary computational approach. Int J Adv Manuf Technol 78(5–8):781–793
17. Chinchanikar S et al (2022) ANN modelling of surface roughness of FDM parts considering the effect of hidden layers, neurons, and process parameters. Advances in Materials and Processing Technologies, ahead-of-print(ahead-of-print): pp 1–11
18. Tayyab M et al (2023) Prediction of mechanical properties for acrylonitrile-butadiene-styrene parts manufactured by fused deposition modelling using artificial neural network and genetic algorithm. Int J Comput Integr Manuf 36(9):1295–1312
19. Alafaghani A et al (2021) Modeling the influence of fused filament fabrication processing parameters on the mechanical properties of ABS parts. J Manuf Process 71:711–723
20. Tura AD et al (2023) Prediction of tensile strength in fused deposition modeling process using artificial neural network and fuzzy logic. Progress in Additive Manufacturing 8(3):529–539
21. Yadav D, Chhabra D, Garg RK, Ahlawat A, Phogat A (2020) Optimization of FDM 3D printing process parameters for multi-material using artificial neural network. Materials Today: Proceedings 21(Part 3):1583–1591. https://doi.org/10.1016/j.matpr.2019.11.225
22. Gurrala PK, Regalla SP (2014) Multi-objective optimisation of strength and volumetric shrinkage of FDM parts A multi-objective optimization scheme is used to optimize the strength and volumetric shrinkage of FDM parts considering different process parameters. Virtual and Physical Prototyping 9(2):127–138
23. Ghiasi H, Pasini D, Lessard L (2011) A non-dominated sorting hybrid algorithm for multi-objective optimization of engineering problems. Eng Optim 43(1):39–59. https://doi.org/10.1080/03052151003739598
24. Selva Rani B, Aswani Kumar C (2015) A comprehensive review on bacteria foraging optimization technique, Springer, Berlin Heidelberg, pp 1–25
25. Selvam A et al (2022) Multi-objective optimization and prediction of surface roughness and printing time in FFF printed ABS polymer. Sci Rep 12(1):16887
26. Raju M et al (2019) A hybrid PSO-BFO evolutionary algorithm for optimization of fused deposition modelling process parameters. J Intell Manuf 30(7):2743–2758
27. Taherdoost H, Madanchian M (2024) A comprehensive survey and literature review on TOPSIS. International Journal of Service Science, Management, Engineering, and Technology 15(1):1–65
28. Dev S, Srivastava R (2023) Influence of process variables on mechanical properties and material weight of acrylic butadiene styrene parts produced by fused filament fabrication. Progress in Additive Manufacturing 8(2):143–158
29. Kamaal M et al (2021) Effect of FDM process parameters on mechanical properties of 3D-printed carbon fibre-PLA composite. Progress in Additive Manufacturing 6(1):63–69
30. Nguyen PQK et al (2022) Predicting material properties of additively manufactured acrylonitrile butadiene styrene via a multiscale analysis process. Polymers (Basel) 14(20):4310. https://doi.org/10.3390/polym14204310
31. Nguyen PQK et al (2024) Influences of printing parameters on mechanical properties of recycled PET and PETG using fused granular fabrication technique. Polymer Testing 132:108390
32. Kechagias JD (2024) 3D printing parametric optimization using the power of Taguchi design: an expository paradigm. Mater Manuf Processes 39(6):797–803

33. Tsiolikas A, Spahiu T, Kechagias JD (2024) Experimental investigation of build time during ABS filament material extrusion process, Springer Nature Switzerland, pp 339–345

34. Abas M et al (2025) Definitive screening design for mechanical properties enhancement in extrusion-based additive manufacturing of carbon fiber-reinforced PLA composite. Prog Addit Manuf 10:139–157. https://doi.org/10.1007/s40964-024-00610-3

35. MATLAB Help Center, fitrnet - Train neural network regression model, since R2021a. https://au.mathworks.com/help/stats/fitrnet.html

36. Katoch S, Chauhan SS, Kumar V (2021) A review on genetic algorithm: past, present, and future. Multimed Tools Appl 80(5):8091–8126

37. Behzadian M et al (2012) A state-of the-art survey of TOPSIS applications. Expert Syst Appl 39(17):13051–13069

38. Alafaghani A, Qattawi A (2018) Investigating the effect of fused deposition modeling processing parameters using Taguchi design of experiment method. J Manuf Process 36:164–174

39. Singh S et al (2019) Mechanical feasibility of ABS/HIPS-based multi-material structures primed by low-cost polymer printer. Rapid Prototyping Journal 25(1):152–161

40. Mohamed OA, Masood SH, Bhowmik JL (2016) Investigation of dynamic elastic deformation of parts processed by fused deposition modeling additive manufacturing. Advances in Production Engineering & Management 11(3):227–238

41. Pazhamannil RV, Govindan P, Sooraj P (2021) Prediction of the tensile strength of polylactic acid fused deposition models using artificial neural network technique. Materials Today: Proceedings 46:9187–9193

42. Pérez M et al (2018) Surface quality enhancement of fused deposition modeling (FDM) printed samples based on the selection of critical printing parameters. Materials 11:11

43. Kumar R et al (2022) Implementation of taguchi and genetic algorithm techniques for prediction of optimal part dimensions for polymeric biocomposites in fused deposition modeling. Int J Biomater 2022:4541450

44. Mohanty A et al (2022) Parametric optimization of parameters affecting dimension precision of FDM printed part using hybrid Taguchi-MARCOS-nature inspired heuristic optimization technique. Materials Today-Proceedings 50:893–903

45. Wankhede V et al (2020) Experimental investigation of FDM process parameters using Taguchi analysis. Materials Today-Proceedings 27:2117–2120

46. Nguyen PQK et al (2024) Study on material behaviours of additively manufactured high-impact polystyrene using artificial neural networks. Prog Addit Manuf 10(2):1461-78

47. Meiabadi MS et al (2021) Modeling the producibility of 3D printing in polylactic acid using artificial neural networks and fused filament fabrication. Polymers (Basel) 13(19):3219

48. Kechagias JD, Chaidas D, Spahiu T (2024) Decorative 3D printing on textiles using elastomer TPU filament under different printing conditions. Rapid Prototyping Journal 30(10):2033–2042